Universal Journal of Civil Engineering
https://ojs.wiserpub.com/index.php/UJCE/

Research Article

Experimental Simulation of Fluidity State Evolution from Slow Earthquake to Strong Earthquake

Lihong Tong[1,2]*, Li Fu[2], Haibing Ding[2]

[1]State key laboratory of performance monitoring and guarantee of rail transportation infrastructure, Nanchang, Jiangxi 330013, China
[2]Institute of Geotechnical Engineering, School of Civil Engineering and Architecture, East China Jiaotong University, Nanchang, Jiangxi 330013, China
E-mail: lhtong@ecjtu.edu.cn

Received: 11 August 2022; **Revised:** 14 October 2022; **Accepted:** 17 October 2022

Abstract: Slow earthquakes have been frequently detected in the neighboring regions of seismogenic zones. However, the physics underlying the connection of slow earthquakes to strong earthquakes remains one of the least understood aspects in seismic research today. By observing the strain time evolution of granular materials in laboratory experiments, we report that the fluidity parameter, which represents a time dependent rate for strain evolution, can be rejuvenated under progressively increasing dynamic loading and this physical quantity finally reaches a critical threshold state, and beyond that catastrophic and uncontained dynamic strain response begins. Moreover, *memory effect* and *anti-fluidization effect* in granular materials are also observed, and these effects underlay the long-term slip events preceded some strong earthquakes, including 2011 M_w 9.1 Tohoku earthquake and 2014 M_w 8.1 Iquique earthquake. The observations indicate the key role of development of fluidity state on connecting slow earthquakes and to full-scale earthquakes.

Keywords: Granular material; Slow earthquake; Fluidity state; Triaxial tests; Dynamics train

1. Introduction

Slow earthquakes are characterized by a mode of slow fault rupture with rate that is insufficient to radiate high-frequency seismic energy [1-3]. These are typically seismic and geodetic events that are characterized by very-low-frequency (less than several Hz) and long durations (days, months to years), respectively [4-8]. There are suggestions that many strong earthquakes are proceeded by an extended nucleation process based on the observation of foreshock sequences and slow earthquakes [7, 9-12]. The characteristic activities of slow earthquakes are believed to have common slip mechanisms to a strong megathrust earthquakes[8]. An insight into the relevance of slow earthquakes to strong earthquakes may provide a useful precursory signal for prediction of impending strong earthquakes. Although the generating mechanism of slow earthquakes has been well investigated [13], the dynamic connecting mechanism of slow earthquakes to strong earthquakes remains elusive [3, 8, 14], that leads to an enigmatic physical origin and controlling mechanics of nucleation process of strong earthquakes [15, 16].

There are many theories and observations on nucleation of earthquakes [15-21] and its connection to slow earthquakes [8, 22-24] has been reported because the significance of slow slip events on understanding or predicting the normal earthquake has been recognized [6]. As the recorded information for 2011 Mw 9.0 Tohoku-oki earthquake is quite complete, a lot of studies have been implemented to learn the knowledge on generation process before the earthquake [25]. The geodetically or seismically observed slow earthquakes [5, 8] may provide a physical insight on some foreshock sequences [10], however, the mechanism of foreshocks to trigger strong earthquakes is still very much unclear. For example, although intense foreshocks and multiple slow-slip events preceded the 2014 Iquique Mw 8.1

DOI: https://doi.org/10.37256/xxxx

earthquake were identified [12, 22], the connecting mechanism of these precursory events to the strong earthquake remains suspending. A number of attempts and intense efforts on modeling the nucleation process of strong earthquakes in theoretical studies [15, 26-29], numerical investigations [17, 30-32] and experiments [3, 16, 33-37] can be found. The theoretical models, however, can be only applicable under specific frictional conditions [27, 28] and a fundamental physical mechanism is still elusive. This is mainly because the preceded slow slip events have been observed under different geologic settings with wide durations [8] which raises the question that whether all these events follow the universal mechanism [3].

The contemporary knowledge on the mechanism of slow earthquakes and its relation to normal earthquakes mainly depends on seismic or geodetic observations [3]. These approaches can only provide a phenomenal and incomplete understanding of the physics while it does not lead to an underlying mechanical explanation for these events. Laboratory earthquake experiments provides alternative method to understand the characteristics of earthquakes and corresponding physical mechanism [38]. However, details and systematic laboratory observations of slow slip events and their relevance to normal earthquakes have been rarely reported. To illuminate the underlying physical mechanism of slow earthquakes, here we describe laboratory experiments that reproduce the transition of slow slip events to rapid slip behavior under geophysical conditions of confining pressure and cyclic loadings. The fault composition is simulated using spherical glass beads, which are frequently selected as the substitution of detritus in fault gouge [19, 33, 39], mainly because the as-fabricated specimen can be easily controlled for quantitative analysis. From our laboratory observations, we find that the increasing dynamic load can promote the granular system to evolve from sable state to fluidic state gradually, which underlies the physical mechanism for the process from slow earthquake to strong earthquake. A memory effect and anti-fluidization effect is also found and this phenomenon provides a reasonable interpretation on the long-term slip events. Generally, the findings in this work provide a possible path to release useful warning information on any imminent earthquake.

2. Methods

2.1. Experimental setup and loading process

Fluidity is one of important parameters that control the rheological behavior in granular materials. A high fluidity state is corresponding to a high strain rate under a specific loading conditions. Inspired by the discovery of sudden increase of slip rate inferred by stress perturbation [24], we strongly suspect that dynamic loadings or vibrations may trigger the fluidity state transition in fault gouge, hence inducing strong earthquakes. Bearing this in mind, we set out to explore experimentally the effect of dynamic loading on strain evolution and further fluidity transition behavior to understand its relevance to earthquakes.

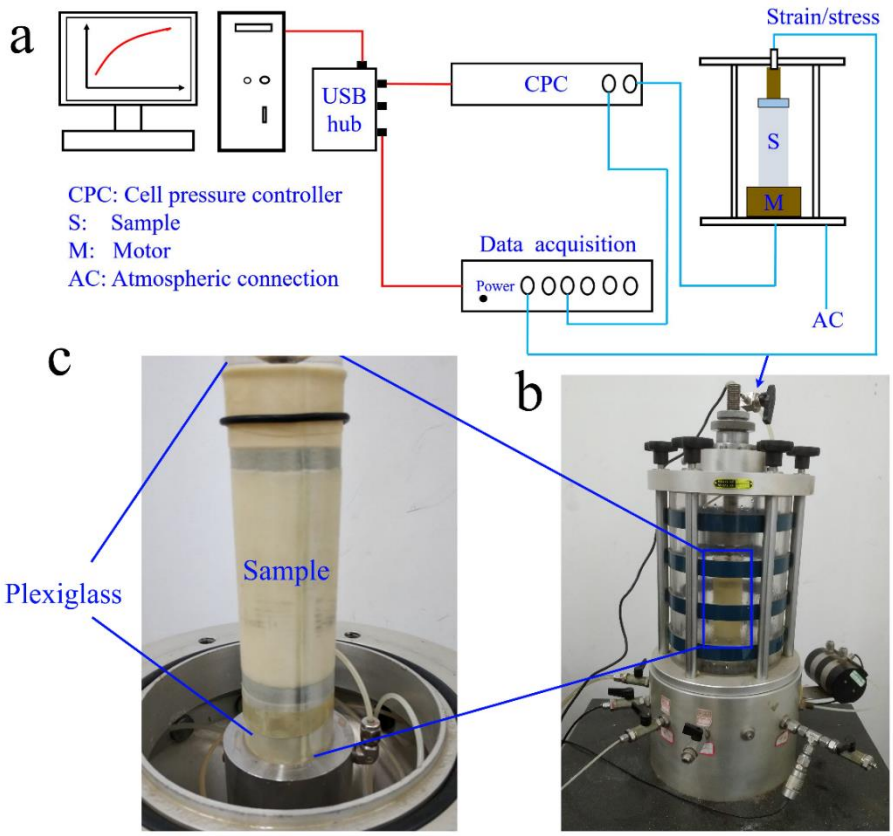

Figure 1. **(a)** The schematic diagram of the dynamic test system. The confining pressure is provided by the cell pressure. The motor can provide normal load and dynamic load with different frequencies and amplitudes. The stress and strain is measured from the gages set on the top of sample cell. The sample is kept atmospheric connection through a pipe during the loading process. **(b)** The device of sample cell used in our tests. **(c)** A typical sample, which is fabricated by glass beads with diameter ranging from 0.2mm to 0.25mm, used for our experimental observations.

Figure 1 shows the schematic diagram of the experimental setup. In our laboratory experiments, the glass beads were selected to simulate the fault composition, which were frequently selected as the substitution of detritus in fault gouge [19, 33]. The diameter of the selected glass beads ranged from 0.2 mm to 0.25 mm. The whole experimental systems are schematically shown in Fig. 1(a). The confinement pressure can be well controlled by the CPC (cell pressure controller) and the axial loads were provided by the motor from the bottom of the sample. For sample preparation, the glass beads were poured into a duralumin cylindrical mold of inner-diameter d=50 mm and filled to a height of h=100 mm (Fig.1(c)). The mold was lined with a latex membrane which was used for confining glass beads after removing the mold. Before removing the mold, the interstitial air was evacuated by a vacuum pump ensuring the sample to be stable. The confined sample was closed hermetically by two fitted plexiglasses at its two end-faces and then mounted to the experiment system.

After the sample was fixed into the pressure cell, a confinement pressure in target value P_0 was applied by injecting the water into the pressure cell. The confining pressure can be accurately adjusted by the CPC (shown in Fig. 1(a)). Then opened the valve of AC pipe to ensure that the applied confinement pressure can be singly and accurately controlled by the CPC. To ensure the sample's equilibrium, the sample was consolidated under the confinement pressure P_0 combined with a deviatoric stress σ_0 (Fig. 2(a)), which simulates the consolidation of fault core under geostatic stress. Here we observed the strain rate within consolidation process to determine whether the system had come into equilibrium. When the strain accumulation within 5 minutes was less than 0.0015%, the system was regarded to enter equilibrium. In order to explore fluidity evolution process of granular materials under dynamic loading, the experiments reported were conducted using two distinct dynamic loading processes: i) applied progressively increased dynamic loads in amplitude and ii) applied alternant amplitude of dynamic loads. The stress and strain during the dynamic loading process were recorded by the stress/strain sensors. Typical cycles of stress and strain signals are shown in Fig.2 (b) and (c).

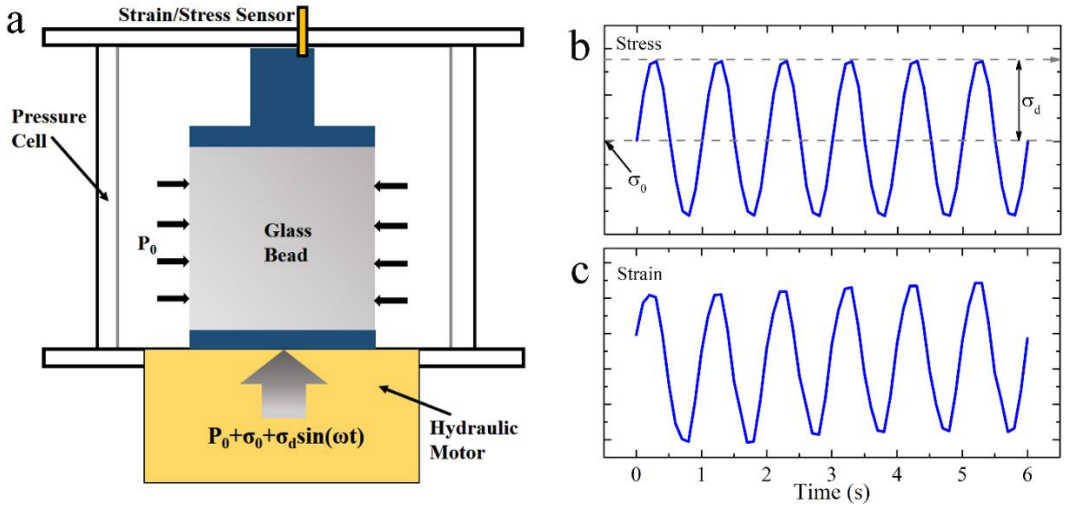

Figure 2. **(a)** Diagram of the set-up and the applied loading conditions: P_0 is the confining pressure, σ_0 is the static deviatric stress, σ_d and ω are dynamic load amplitude and circular frequency, respectively. **(b)** Dynamic load signal measured directly by the stress sensor. **(c)** Typical strain response signal under dynamic loading recorded by the strain sensor.

2.2. Conversion of measured strain to fluidity parameter

To analyze the fluidity state in a certain dynamic loading process, the fluidity parameter is introduced as $D = G/\eta$ with G and η are shear modulus and effective viscosity of the material, respectively, which is followed by the work of Derec et al. [40], then the dynamics of fluidity *D* coupling with strain rate can be given by a simple and lower order coupling equation within the framework of complex rheology as

$$\dot{D} = -rD^2 + u\dot{\gamma}^2, \quad \dot{\sigma} = -D\sigma + G\dot{\gamma} \tag{1}$$

where γ is the shear strain, r and u are the aging parameters and rejuvenation parameter, respectively, $\sigma = \sigma_0 + \sigma_d \sin(\omega t)$ is the deviatoric stress with σ_d and ω the amplitude and circular frequency of dynamic loads, respectively. Eq. (1) can be solved numerically by set the specific initial conditions on strain and it can be found that the shear strain is fluctuated with time.

To verify the theoretical model, a static deviator stress $\sigma_0 = 167\,\mathrm{kPa}$ coupled with a confining pressure 0.3 MPa was applied to the fabricated sample. After the sample coming into steady state, a dynamic load with amplitude $\sigma_d = 23.3\,\mathrm{kPa}$ and frequency 1 Hz was applied, and the dynamic load is maintained for 2500 cycles. We choose 8 cycles to representatively show the stress-strain relation (Fig. 3(a)) and apparent strain accumulation can be captured. The strain evolution for the whole dynamic loading duration is shown by Fig. 3(b), which can be exactly predicted by Eq. (1) if proper parameter on *r* and *u* are selected (the parameters selection will be discussed in next section). Within one cycle, the shear strain is fluctuated due to the dynamic load as shown by the inset of Fig. 3(b). However, we find that the shear strain accumulation exhibits logarithmic relation with time which can be well represented by the envelope of strain-time evolution. In this consideration and for clarity, representative data can be extracted with 1s interval from the strain-time evolution to fully show the strain accumulation during the dynamic loading as shown by the red data point in inset of Fig. 3(b). Therefore, we can reasonably assume that the dynamic deviatoric stress is supposed to have only influence on the mechanical properties such as viscosity, modulus and so on, and the strain accumulation is induced by the static deviatoric stress because of the increase in fluidity of granular material under dynamic loading. As a result, only the static part σ_0 of deviatoric stress σ in Eq. (1) is considered and further to give that $\dot{\sigma} = 0$.

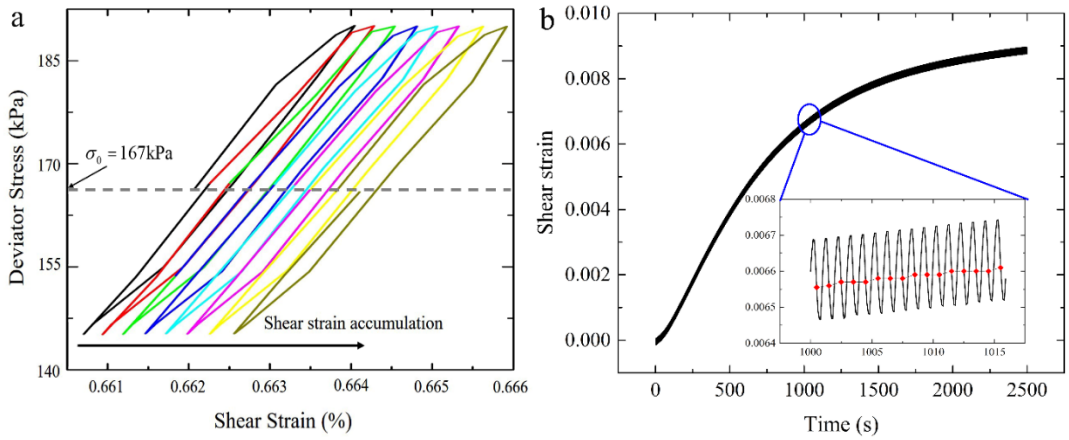

Figure 3. **(a)** A typical stress-strain relation to show the shear strain accumulation under dynamic loading. **(b)** A representative shear strain evolution with time. The inset is partly enlarged from the strain evolution to show the strain perturbation under dynamic loading. The red data point is extracted with 1s interval to clearly show the strain accumulation with time. For both (a) and (b), the confining pressure is set as 0.3 MPa, the static deviatric stress $\sigma_0 = 167\,\mathrm{kPa}$, the dynamic load amplitude is $\sigma_d = 23.3\,\mathrm{kPa}$ and the load frequency 1 Hz.

In consideration of above discussion and following the mathematical manipulation in the work of Espíndola et al. [41], Eq. (1) can be easily solved as

$$\gamma(t) - \gamma_0 = \frac{\sigma_0}{aG}\ln\left[1 + aD_0\left(t - t_0\right)\right] \tag{2}$$

Where t_0 is start-time of each dynamic process, γ_0 and D_0 are the initial strain and initial fluidity parameter at each loading process, respectively, a is an effective aging parameter which is defined as $a = r(1-\sigma_0^2/\sigma_D^2)$ with $\sigma_D = \sqrt{r/u}G$. As the initial fluidity parameter D_0 can be determined from the initial slope of strain time evolution, $D_0 = G\left(\dot{\gamma}\big|_{t=t_0}\right)/\sigma_0$, the effective aging parameter is the only adjustable parameter to fit the experimental data. From Eq. (2), the fluidity parameter evolution can be further given as

$$D(t) = \frac{D_0}{1 + aD_0(t - t_0)} \tag{3}$$

It should be remarked here that Eq. (2) is obtained on the basis of which shear modulus is constant. In fact, the system has been observed to be softened under dynamic loading [33]. The relative change in modulus is less than 10% even when the input dynamic loading amplitude increases by two orders of magnitude as shown by the experimental observations in the work of Johnson and Jia [33]. However, the relative change in effective viscosity can be as high as two orders of magnitude even for dynamic load amplitude increases by several times [41]. Thus the influence of modulus change on fluidity parameter is significantly small compared with that of effective viscosity on fluidity parameter. As a result, the assumption on constant modulus has insignificant influence on fluidity state analysis.

3. Results

3.1. Fluidity state under progressively increased dynamic loading

In the earth, the fault core may be in a complex field geological conditions (pore pressure, temperature, tectonic stress, etc.) and also be impacted by different types of waves. To focus our concerns on whether the fluidity state of the granular material is effected by dynamic loading, we only partially reproduce the field confining pressure and limit our investigations to single-frequency (1 Hz) axial cyclic dynamic load with amplitude σ_d. At first, we performed experiments to capture the shear strain evolution characteristics of granular material with a progressively increasing dynamic loads. The continuously applied dynamic loading is analogous to a field condition in which continuous foreshocks preceded a strong earthquake, for example the 2011 M_w 9.0 Tohoku earthquake [11, 25, 42] and 2014 Iquique M_w 8.1 earthquake [12, 42]. Fig. 4(a) shows the strain evolution in the glass bead packing under $P_0 = 0.3\,\mathrm{MPa}$ confinement pressure and 163 kPa deviatoric stress ($\sigma_0 = 163\,\mathrm{kPa}$). After 1.8 hours of pre-consolidation to guarantee a steady state for the sample (see the inset of Fig. 4(a)), seven progressively increasing dynamic

loads with amplitude starting from 23.3 kPa in an increment 14 kPa were applied successively and a 2500s of duration for each process (except the last process in which failure occurred) was maintained. For clarity, we have extracted representative data with 1s interval (see the inset of Fig. 3(b)) to observe the strain evolution, which is shown in Fig. 4(a) for the whole loading process. Skips in strain rate is obviously observed to accelerate the strain accumulation once the dynamic load amplitude is increased, indicating a gradual fluidity state transition in the granular material. Fig. 4(b) shows the continuous evolution of fluidity parameter from jammed state (steady state) to fluidic state (stage vii in Fig. 4(a)). Before the appearance of dynamic loads, the granular system exhibits a jammed state on which no further strain is accumulated. Once the dynamic load appears, an abrupt increase in fluidity parameter is observed, indicating the system has entered into the transition state. When the dynamic load is maintained at a constant amplitude, the system is gradually aged as clearly shown in Fig. 4(b). However, when a dynamic load with larger amplitude is applied, the initial fluidity parameter D_0 jumps to a higher value as shown by Fig. 4(c), indicating a stepping rejuvenation of the system. Once the fluidity parameter beyond the critical fluidity state, the strain in granular system continuously develops, implying that the system transfers into a fluidic state (stage vii shown in Fig. 4 (b)). For the whole loading process, we also present the effective aging parameter evolution in Fig. 4(d), finding that it keeps constant in each stage while steps to decrease with increasing dynamic load amplitude. This is also a representation of evolution of fluidity state as the effective aging parameter reduces to zero when the system comes into fluidic state.

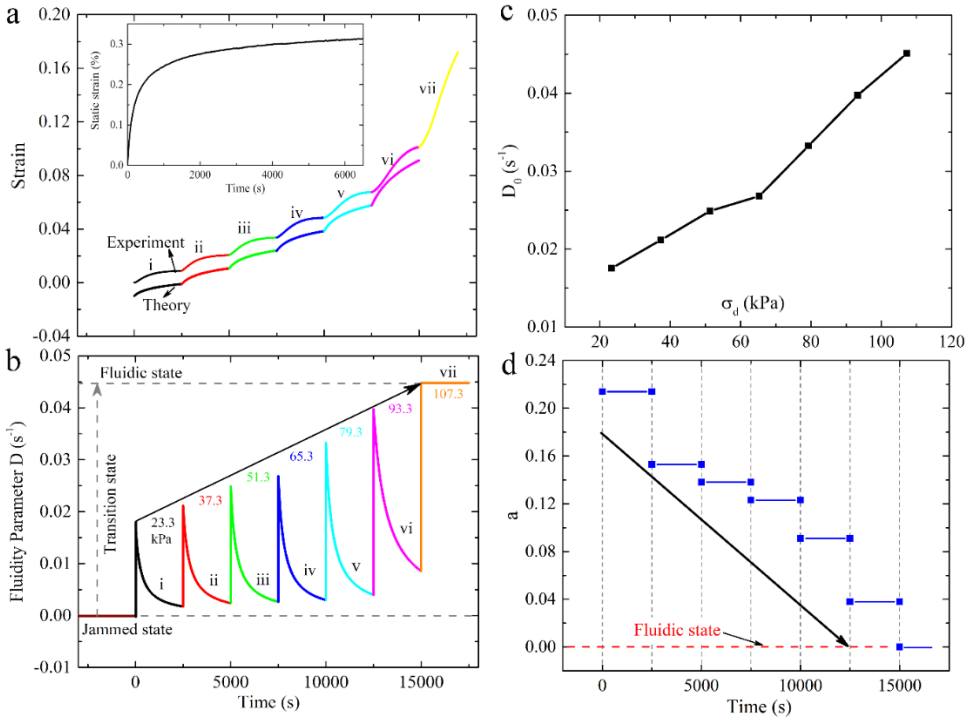

Figure 4. Fluidity state evolution due to dynamic loading. **(a)** Experimentally measured and fitted strain evolution under progressively increased dynamic loads. The applied confinement pressure is $P_0 = 0.3\,\mathrm{MPa}$ and the static deviatoric stress $\sigma_0 = 163\,\mathrm{kPa}$. The up-left inset shows the method for extracting representative data. The down-right inset shows the pre-consolidation stage ensuring an equilibrium before dynamic loading. **(b)** Evolution of fluidity parameter corresponding to the dynamic loading processes in (a). The numbers shown in each process is the dynamic load amplitude. The frequency of dynamic load is maintained at 1 Hz. The horizontal coordinate is shared with (a). **(c)** Initial fluidity parameter D_0 in each loading process. **(d)** Step decrease of effective aging parameter a during the fluidity state transition.

We believe that the experimentally observed fluidity evolution described in Fig. 4(b) well underlies the state developing of the material in fault core preceding some large earthquakes, before which intense foreshocks have been observed such as the 2011 Mw 9.0 Tohoku earthquake [11] and 2014 Iquique Mw 8.1 earthquake [12]. In the vicinity of earthquake hypocenter, materials in the fault may be suspected to have experienced the same fluidity transition process under dynamic loads induced by foreshocks. The vibrations induced by the foreshocks propagate into the seismogenic zone to propel the material in fault core from jammed state into fluidic state, finally leading to a strong earthquake. This physical understanding also provides an insight on the dynamic triggering at remote distance such as 1999 M7.1 Hector Mine[43] and the 2002 M7.9 Denali [44]. Some huge land sliding induced by the mainshocks or aftershocks may also share the same physical mechanism of fluidity state transition induced by dynamic

loading [45-47].

3.2. Fluidity state evolution under alternant amplitude of dynamic loading

A very long-term slow slip event preceding the 2011 Tohoku earthquake (January 2002 to 8 March 2011) has been reported in the Japan trench subduction zone [7]. To explore and understand the slow slip event, we performed the strain evolution experiment by applying dynamic loads with alternant amplitudes to characterize the fluidity state development. The strain evolution under a specifically designed loading process is illustrated in Fig. 5. The static deviatoric stress and confinement pressure were enhanced to 233 kPa and 0.4 MPa, respectively. A 2 hours pre-consolidation was implemented under the confining pressure 0.4 MPa to ensure a steady state before applying dynamic loads (this process is not shown out).

The applied dynamic load amplitudes are shown in the inset of Fig. 5(a). The dynamic loading processes can be divided into three phases as shown in Fig. 5. In each phase the dynamic load amplitude is progressively increased. Phase 1 is same to that described in Fig. 4, showing nothing new. At the initial process of phase 2, we remove the dynamic load to let the system be under static load, finding that the fluidity state returns to jammed state and no strain accumulation develops, implying a significance of dynamics on fluidity rejuvenation. When the dynamic loads with amplitudes of 74.64 kPa and 93.3 kPa are repeated in phase 3 (stages Vii and Viii), no fluidity state skip appears as shown by the inset of Fig. 5(b), meaning that the granular material has a '*memory effect'*, of which fluidity state remains under dynamic loads with amplitudes that ever experienced by the material. The system is almost not affected even when the dynamic load amplitude is further enhanced to 116.525 kPa (stage ix), implying a strengthened resistance in fluidization after repetitive dynamic loading. However, when a high enough dynamic load comes, which is analogous to the dynamic loads induced by the intense foreshocks preceding to large earthquakes in field condition, an abrupt large skip in fluidity parameter occurs to suddenly propel the system to fluidic state, implying a large earthquake occurs.

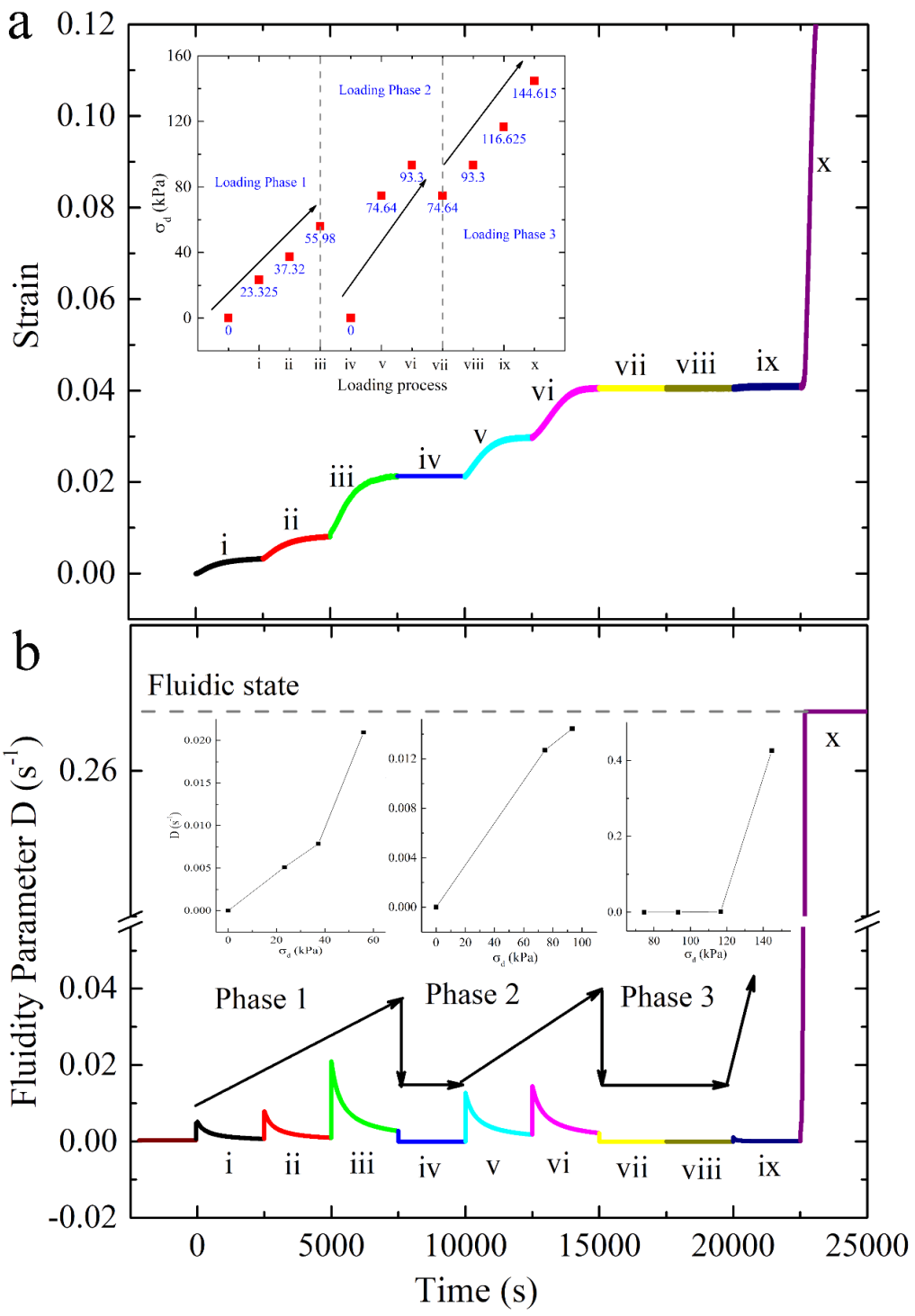

Figure 5. Fluidity state evolution under dynamic loads with alternant amplitudes at 0.4 MPa confining pressure. (a) Strain evolution. The inset shows the dynamic load amplitude in each loading process. The deviatoric stress is 233 kPa. The pre-consolidation process under static load is persisted for 2 hours to ensure a state of equilibrium. The applied dynamic load frequency is 1 Hz. (**b**) Evolution of fluidity state corresponding to the loading processes in (a). The insets show the initial fluidity parameter D_0 in each phase. The horizontal coordinate is shared with (a).

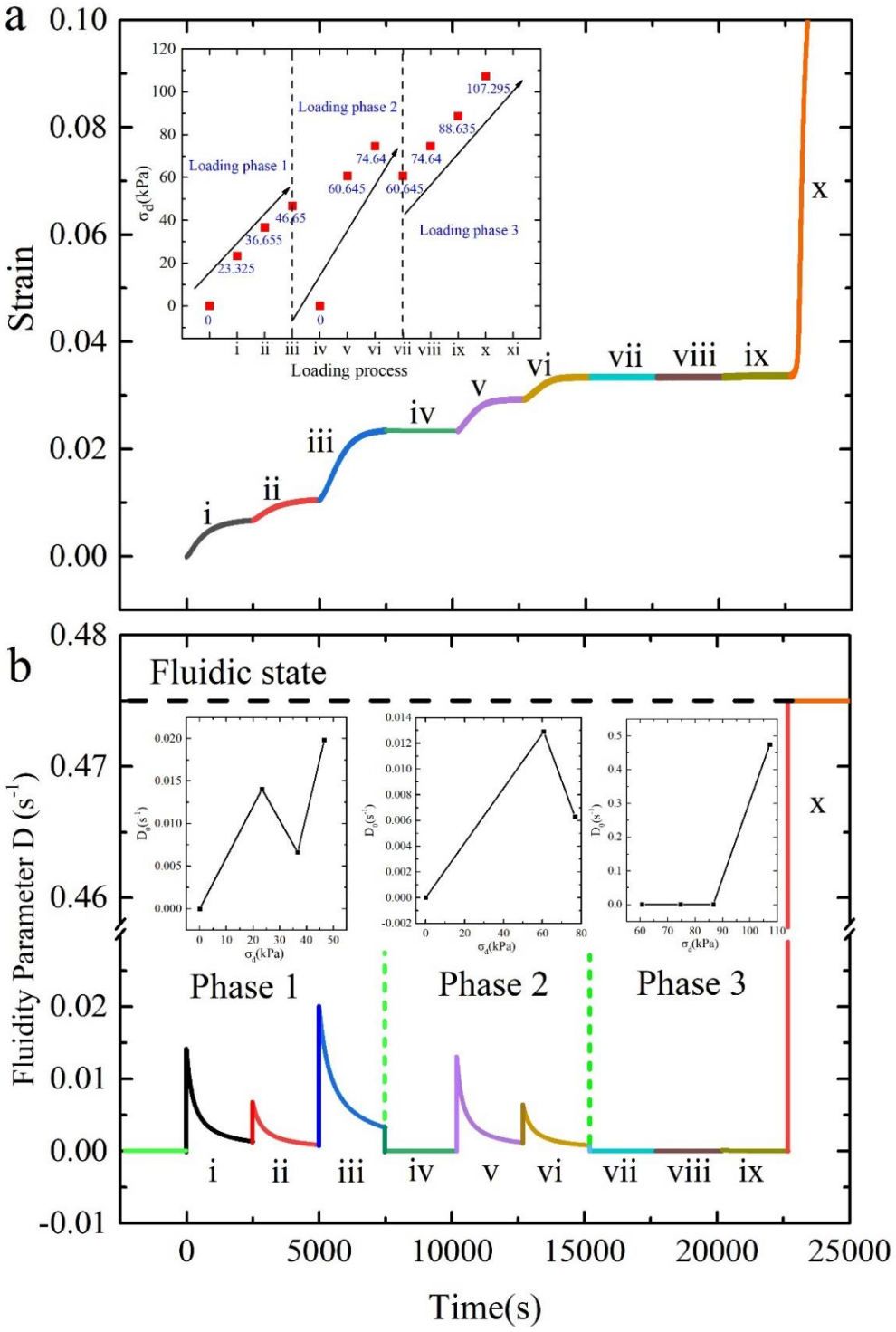

Figure 6. Fluidity state evolution under dynamic loads with alternant amplitudes at 0.3 MPa confining pressure. (a) Strain time evolution. The inset shows the dynamic load amplitude in each loading process. The deviatoric stress is 163 kPa. The pre-consolidation process under static load is persisted for 2 hours to ensure a state of equilibrium. The applied dynamic load frequency is 1 Hz. (**b)** Evolution of fluidity state corresponding to the loading processes in (a). The insets show the initial fluidity parameter D_0 in each phase. The horizontal coordinate is shared with (a).

A same experimental result by reducing the confinement pressure to 0.3 MPa and static deviatoric stress to 163 kPa is shown in Fig. 6. The *memory effect* can also be observed but the system shows a more complex fluid rheology. The initial fluidity parameter $_{D_0}$ does not exhibit a monotonically increasing trend with increasing dynamic load amplitude in each phase as shown by the insets of Fig. 6(b), but the global fluidity transition of the system keeps consistent to that described in Fig. 5. We, again, find that after repeating the dynamic loads which the system has ever experienced, the fluidity state of the system

cannot be significantly enhanced by applying a relative high dynamic load (see stage ix in Fig. 6), which further supports our hypothesis that repetitive dynamic loading has a strengthening effect on *anti-fluidization*. However, when a high enough load is followed (stage x in Fig. 6), the system suddenly falls into fluidic state, following the ruptures. Although the fluidity state evolutions described in both Figs. 5 and 6 are different from that in Fig .3 due to the different dynamic loading methods, the rupture mechanism of high fluidity state is shared by them. However, we do not yet fully understand the micro physical mechanism for the difference of fluidity state evolution under different loading processes. Maybe the frictional slip dynamics [34] of micro-contacts of grains can give a fundamental understanding, on which we will pay further effort in our future works.

4. Discussion

4.1. *Interpretation on dynamic memory effect*

To understand the *memory effect*, we introduce a statistical model to give a conceptual interpretation. Assume that each grain contact is in a certain stress-strain state under a specific external condition and all these states assemble to the system in most probable way. Suppose that the grains can slide at the contact when the applied load amplitude σ_d beyond a certain value, reading as critical sliding stress σ_c, and the distribution of value of σ_c can be verified to satisfy a certain distribution law (here we select the Maxwell distribution [48, 49], other distribution laws, for example Gaussian distribution, are possible, but this form is the most likely one for most probable distribution problems), which is schematically shown in Fig. 7. In fact, the form of selected distribution law has no influence on understanding the physical mechanism of *memory effect*. If a dynamic load with amplitude σ_{d0} appears (for example, stage vi in Fig. 5), the grain contacts on state that less than σ_{d0} (i.e. $\sigma_c < \sigma_{d0}$) will slide. However, the grains cannot move fast enough to relax the full strain within on cycle of loading, hence inducing the macro creep. When the strain is fully relaxed, all the sliding contacts reach a higher critical sliding state than σ_{d0} (a stable state under impacting dynamic load σ_{d0}). Then if a dynamic load with amplitude less than σ_{d0} is repeatedly applied on the system (for example stages vii and viii in Fig. 5 and Fig. 6), no grains can slide as no critical sliding stress less than σ_{d0}, performing a *memory effect* (schematically shown in Fig. 7). If the dynamic load is progressively increased, number of sliding grains is also progressively increased and continuous strain accumulation can be induced (the case presented in Fig. 4). When the applied dynamic load reaches a critical value, reading as critical fluidic load σ_{d_c}, enough amount of contacts slide, and the system thus falls into fluidic state. It should be noted that, in this work we focus on presenting the fundamental physical mechanism, hence the quantitative analysis is not elaborated. A quantitative analysis can be found in our previously published work [48], in which a statistical model to predict the softening effect is proposed and the corresponding fluidization evolution is also quantitatively studied.

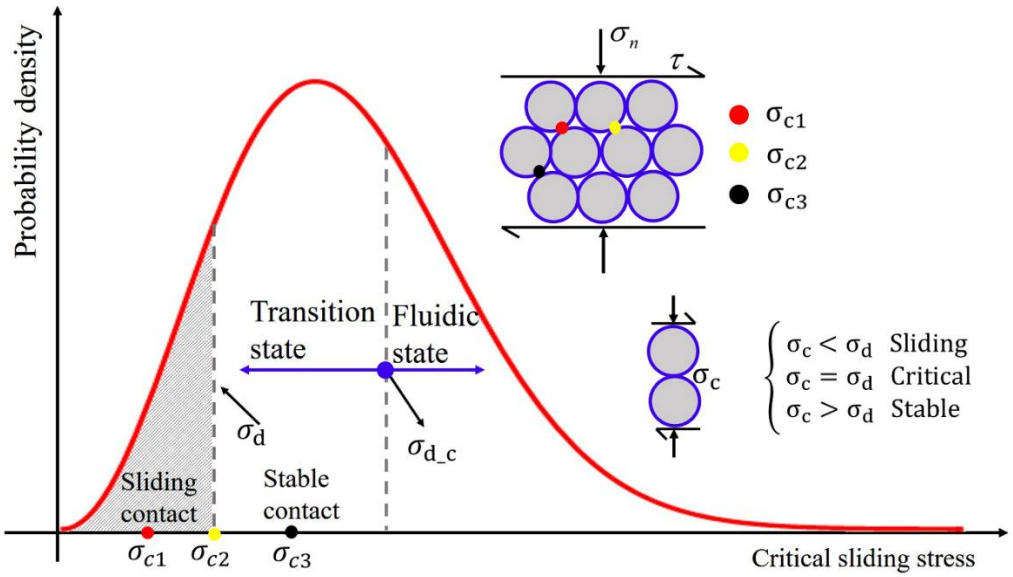

Figure 7. Representation of "*memory effect*" and fluidity state transition. σ_c is critical stress that the grain contact can sustain

to keep stable. σ_d is the dynamic load amplitude. The hatched area stands for the fraction of sliding contacts under dynamic load with amplitude σ_d and it increases with the progressively increased applied dynamic. σ_{d_c} is critical fluidic load beyond which the system comes into fluidic state.

4.2. Understand connection of slow earthquakes to large earthquakes

Based on the previous discussions on fluidity development and interpretation on *memory effect* of granular material under dynamic loading, we are able to fully comprehend the physics underlying a long-term slip event preceded the 2011 Tohoku earthquake. Before 16 February 2011, the shear strain in seismogenic zone is slowly accumulated by scattering dynamic loads propagated from neighboring region (schematically shown by Fig. 8). However, bulk fluidity state transition rate is rather low due to small amount of events and the lacking in high amplitude dynamic loads. Therefore, the fluidity state of the material in seismogenic zone is far below the critical state. Meantime, the material may have experienced many times of repetitive dynamic loading, which strengthened the resistance in fluidization. Both the *memory effect* and *anti-fluidization effect* make the fault undergo a long slow slip process. There was a sudden increase in the rate of activity in the neighboring region of hypocenter on 16 February 2011, nearly 24 days before the earthquake [11] and it persisted for 12 days, and thus it induced the first fast fluidity state transition. After a 9-day seismic quiescence period (the fault returned to jammed state in this period as no dynamic loads further appeared), an intense foreshock activity started on 9 March, two days before the megathrust, including an M_w 7.3 shock, which resulted in higher amplitude of dynamic loads due to the wave interference. When the dynamic loads induced by the foreshocks impacted on the material in seismogenic zone, the second fast fluidity state transition was incurred until the critical state came, and following the megathrust. The fluidity state evolution before the Tohoku earthquake is schematically recovered in Fig. 8(b). Like the Tohoku earthquake, intense foreshocks activity began on 4 January 2014 that were almost three months preceded the megathrust of the 2014 M_w 8.1 Iquique earthquake [12, 42]. We believe that the hypocenter region of the 2014 Iquique earthquake may also have undergone a similar behavior as that in the 2011 Tohoku earthquake, in which sparse events induced slow fluidity state transition in the preliminary process and the subsequent rapid state transition was caused by the intense foreshocks until the arrival of the critical state, and the ultimate megathrust.

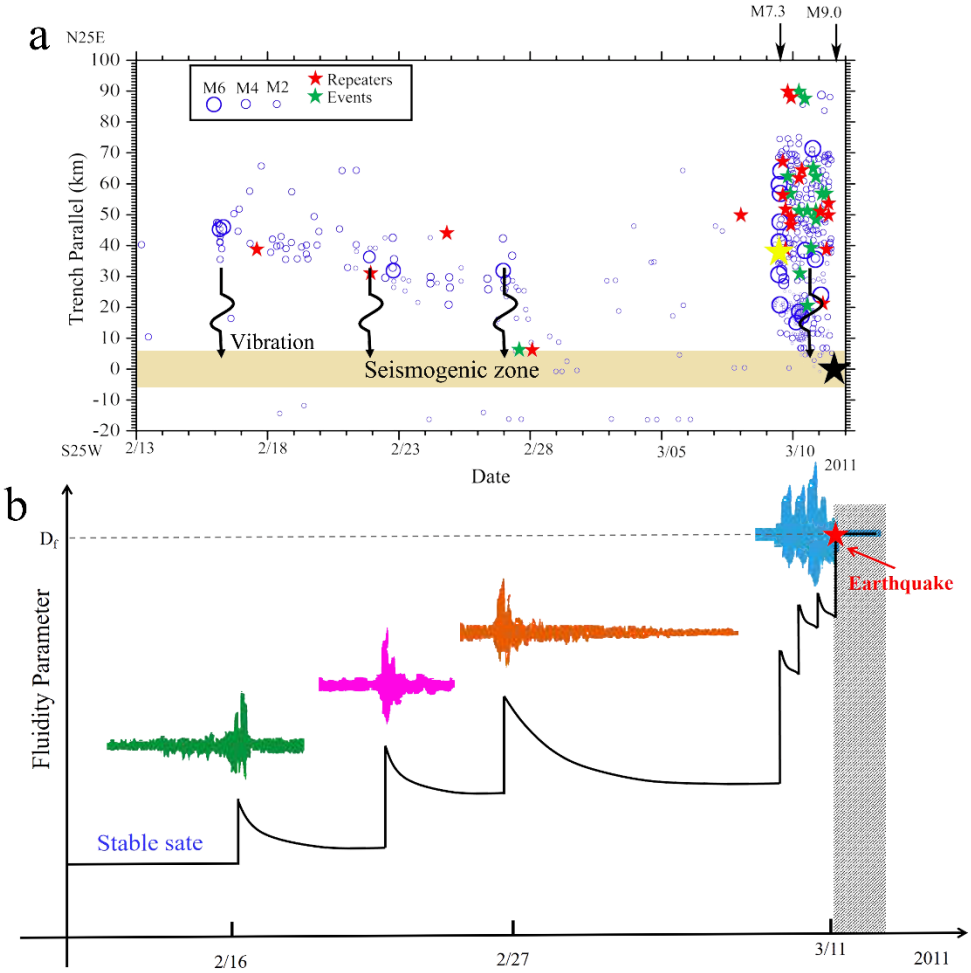

Figure 8. Schematic of dynamic triggering of the 2011 Tohoku M_w 9.1 earthquake. (a) Space-time diagram of detected events between 13 February and megathrust origin time (partly reproduced from *Figure 2* in Ref. [11]). The yellow star denotes the M_w 7.3 largest foreshock while the black star denotes the M_w 9.1 mainshock. **(b)** Schematic figure that reproduces the fluidity state transition in hypocenter region induced by dynamic loading corresponding to the foreshocks preceded the megathrust in (a).

5. Conclusions

From our laboratory observations, we have conducted a detailed analysis the fluidity evolution characteristics of granular material under different dynamic loading conditions. With an increase in dynamic load amplitude, the granular material undergoes fluidity development from jammed state stepping to the fluidic state and finally the failure occurs. If the dynamic loads with high-low alternant amplitudes are applied, a *memory effect* and *anti-fluidization effect* can be observed. A statistic model has been employed to give an interpretation on this phenomenon. Based on the analysis in this work, we find that the fluidity state evolution underlies a plausible inducing mechanism of normal earthquakes by foreshocks. Furthermore, the *memory effect* and *anti-fluidization effect* combined with fluidity state evolution provides a reasonable interpretation on the long-term slip events. Therefore, the fluidity state can bridge physical mechanism of the long-term slip events to a normal earthquake. In general, we can summarize the necessary conditions for triggering of strong earthquakes as: first a seismogenic zone; next dynamic loads with an amplitude higher than that experienced in the seismogenic zone; and finally reaching fluidic state. Thus, a long-term monitor of slow earthquake activity in subduction zone is able to provide important and beneficial information for evaluating the development of seismogenic zone in fluidity state. Consequently, the degree of criticality in any earthquake-prone region neighboring to slow earthquake sources may provide useful warning information on any imminent earthquake and to help the mitigation of the aftermath that involves devastating and catastrophic damages. However, with appearance of water in the fault, the role of pore pressure and temperature in deep underground is still an open and challenging issue and further examining their interactions is beneficial to contribute deeper understanding of the evolution mechanism from slow earthquake to strong earthquake.

Acknowledgments

This work is supported by the National Natural Science Foundation of China (No. 52168049), the Natural Science Foundation of Jiangxi Province (No. 20212BDH81034) and the Fund from education department of Jiangxi province (No. GJJ210618).

References

[1] A.T. Linde, M.T. Gladwin, M.J.S. Johnston, R.L. Gwyther, R.G. Bilham. A slow earthquake sequence on the San Andreas fault. *Nature*. 1996; 383(6595): 65-68.

[2] K. Obara. Nonvolcanic deep tremor associated with subduction in southwest Japan. *Science*. 2002; 296(5573): 1679-1681.

[3] J.R. Leeman, D.M. Saffer, M.M. Scuderi, C. Marone. Laboratory observations of slow earthquakes and the spectrum of tectonic fault slip modes. *Nat Commun*. 2016; 7.

[4] G. Rogers, H. Dragert. Episodic tremor and slip on the Cascadia subduction zone: the chatter of silent slip. *Science*. 2003; 300(5627): 1942-1943.

[5] S. Ide, G.C. Beroza, D.R. Shelly, T. Uchide. A scaling law for slow earthquakes. *Nature*. 2007; 447(7140): 76-79.

[6] Z. Peng, J. Gomberg. An integrated perspective of the continuum between earthquakes and slow-slip phenomena. *Nat Geosci*. 2010; 3(9): 599-607.

[7] Y. Yokota, K. Koketsu. A very long-term transient event preceding the 2011 Tohoku earthquake. *Nat Commun*. 2015; 6.

[8] K. Obara, A. Kato. Connecting slow earthquakes to huge earthquakes. *Science*. 2016; 353(6296): 253-257.

[9] D.A. Dodge, G.C. Beroza, W.L. Ellsworth. Detailed observations of California foreshock sequences: Implications for the earthquake initiation process. *Journal of Geophysical Research Solid Earth*. 1996; 101(B10): 22371-22392.

[10] M. Bouchon, H. Karabulut, M. Aktar, S. Özalaybey, J. Schmittbuhl, M.-P. Bouin. Extended Nucleation of the 1999 Mw 7.6 Izmit Earthquake. *Science*. 2011; 331(6019): 877-880.

[11] A. Kato, K. Obara, T. Igarashi, H. Tsuruoka, S. Nakagawa, N. Hirata. Propagation of Slow Slip Leading Up to the 2011 M-w 9.0 Tohoku-Oki Earthquake. *Science*. 2012; 335(6069): 705-708.

[12] S. Ruiz, M. Metois, A. Fuenzalida, J. Ruiz, F. Leyton, R. Grandin, C. Vigny, R. Madariaga, J. Campos. Intense foreshocks and a slow slip event preceded the 2014 Iquique M-w 8.1 earthquake. *Science*. 2014; 345(6201): 1165-1169.

[13] K. Okazaki. I. Katayama. Slow stick slip of antigorite serpentinite under hydrothermal conditions as a possible mechanism for slow earthquakes. *Geophysical Research Letters*. 2015; 42(4): 1099-1104.

[14] A. Kato, Y. Ben-Zion. The generation of large earthquakes. *Nature Reviews Earth & Environment*. 2021; 2(2): 26-39.

[15] C. Tape, S. Holtkamp, V. Silwal, J. Hawthorne, Y. Kaneko, J.P. Ampuero, C. Ji, N. Ruppert, K. Smith, M.E. West. Earthquake nucleation and fault slip complexity in the lower crust of central Alaska. *Nat Geosci*. 2018; 11(7): 536-541.

[16] B.A. Verberne, J.Y. Chen, A.R. Niemeijer, J.H.P. de Bresser, G.M. Pennock, M.R. Drury, C.J. Spiers. Microscale cavitation as a mechanism for nucleating earthquakes at the base of the seismogenic zone. *Nat Commun*. 2017; 8(1645).

[17] Y. Kaneko, P. Ampuero J. A mechanism for preseismic steady rupture fronts observed in laboratory experiments. *Geophysical Research Letters*. 2011; 38: L21307.

[18] B. Schurr, G. Asch, S. Hainzl, J. Bedford, A. Hoechner, M. Palo, R. Wang, M. Moreno, M. Bartsch, Y. Zhang. Gradual unlocking of plate boundary controlled initiation of the 2014 Iquique earthquake. *Nature*. 2014; 512(7514): 299-302.

[19] P.A. Johnson, J. Carmeliet, H.M. Savage, M. Scuderi, B.M. Carpenter, R.A. Guyer, E.G. Daub, C. Marone. Dynamically triggered slip leading to sustained fault gouge weakening under laboratory shear conditions. *Geophysical Research Letters*.2016; 43(4); 1559-1565.

[20] M. Ahmadi, M. Moosavi, M.K. Jafari. Experimental investigation of reverse fault rupture propagation through wet granular soil. *Engineering Geology*. 2018; 239: 229-240.

[21] S. Ide. Frequent observations of identical onsets of large and small earthquakes. *Nature*. 2019;

573(7772): 112-116.
[22] A. Kato, S. Nakagawa. Multiple slow-slip events during a foreshock sequence of the 2014 Iquique, Chile Mw 8.1 earthquake. *Geophysical Research Letters*. 2015;41(15): 5420-5427.
[23] A.P. Mavrommatis, P. Segall, N. Uchida, K.M. Johnson. Long-term acceleration of aseismic slip preceding the Mw 9 Tohoku-oki earthquake: Constraints from repeating earthquakes. *Geophysical Research Letters*. 2016; 42(22): 9717-9725.
[24] N. Uchida, T. Iinuma, R.M. Nadeau, R. Burgmann, R. Hino. Periodic slow slip triggers megathrust zone earthquakes in northeastern Japan. *Science*. 2016; 351(6272): 488-492.
[25] N. Uchida, R. Bürgmann. A Decade of Lessons Learned from the 2011 Tohoku-Oki Earthquake. *Reviews of Geophysics*. 2021; 59(2): e2020RG000713.
[26] M. Campillo, I.R. Ionescu. Initiation of antiplane shear instability under slip dependent friction. *Journal of Geophysical Research Solid Earth*. 1997; 102(B9): 20363-20371.
[27] J. Chen, C.J. Spiers. Rate and state frictional and healing behavior of carbonate fault gouge explained using microphysical model. *Journal of Geophysical Research Solid Earth*. 2016; 121(12): 8642-8665.
[28] P. Segall, A.M. Rubin, A.M. Bradley, J.R. Rice. Dilatant strengthening as a mechanism for slow slip events. *Journal of Geophysical Research Solid Earth*. 2010; 115: B12305.
[29] M.J. Ikari, C. Marone, D.M. Saffer, A.J. Kopf. Slip weakening as a mechanism for slow earthquakes. *Nat Geosci*. 2013; 6(6): 468-472.
[30] N. Lapusta, J.R. Rice. Nucleation and early seismic propagation of small and large events in a crustal earthquake model. *Journal of Geophysical Research Solid Earth*. 2003; 108(B4).
[31] A.M. Rubin, J.P. Ampuero. Earthquake nucleation on (aging) rate and state faults. *Journal of Geophysical Research Solid Earth*. 2005; 110(B11): B11312.
[32] B. Ferdowsi, M. Griffa, R.A. Guyer, P.A. Johnson, C. Marone, J. Carmeliet. Acoustically induced slip in sheared granular layers: Application to dynamic earthquake triggering. *Geophysical Research Letters*. 2016; 42(12): 9750-9757.
[33] P.A. Johnson, X. Jia. Nonlinear dynamics, granular media and dynamic earthquake triggering. *Nature*. 2005; 437(7060): 871-874.
[34] O. Bendavid, G. Cohen, J. Fineberg. The dynamics of the onset of frictional slip. *Science*. 2010; 330(6001): 211-214.
[35] S. Nielsen, J. Taddeucci, S. Vinciguerra. Experimental observation of stick-slip instability fronts. *Geophysical Journal International*. 2010; 180(2): 697-702.
[36] G.C. Mclaskey, B.D. Kilgore. Foreshocks during the nucleation of stick-slip instability. *Journal of Geophysical Research Solid Earth*. 2013; 118(6): 2982-2997.
[37] S. Latour, A. Schubnel, S. Nielsen, R. Madariaga, S. Vinciguerra. Characterization of nucleation during laboratory earthquakes. *Geophysical Research Letters*. 2013; 40(19): 5064-5069.
[38] D.C. Bolton, S. Shreedharan, G.C. McLaskey, J. Rivière, P. Shokouhi, D.T. Trugman, C. Marone. The High-Frequency Signature of Slow and Fast Laboratory Earthquakes. *Journal of Geophysical Research: Solid Earth*. 2022; 127(6): e2022JB024170.
[39] J. Rivière, Z. Lv, P.A. Johnson, C. Marone. Evolution of b -value during the seismic cycle: Insights from laboratory experiments on simulated faults. *Earth & Planetary Science Letters*. 2018; 482: 407-413.
[40] C. Derec, A. Ajdari, F. Lequeux. Rheology and aging: A simple approach. *The European Physical Journal E*. 2001; 4(3): 355-361.
[41] D. Espíndola, B. Galaz, F. Melo. Ultrasound induces aging in granular materials. *Physical Review Letters*. 2012; 109(15): 158301.
[42] M. Bouchon, D. Marsan, V. Durand, M. Campillo, H. Perfettini, R. Madariaga, B. Gardonio. Potential slab deformation and plunge prior to the Tohoku, Iquique and Maule earthquakes. *Nat Geosci*. 2016; 9(5): 380-383.
[43] J. Gomberg, P.A. Reasenberg, P. Bodin, R.A. Harris. Earthquake triggering by seismic waves following the Landers and Hector Mine earthquakes. *Nature*. 2001; 411(6836): 462-466.
[44] J. Gomberg, P. Bodin, K. Larson, H. Dragert. Earthquake nucleation by transient deformations caused by the M = 7.9 Denali, Alaska, earthquake. *Nature*. 2004; 427(6975): 621-624.
[45] J. Luo, X. Pei, S.G. Evans, R. Huang. Mechanics of the earthquake-induced Hongshiyan landslide in the 2014 Mw 6.2 Ludian earthquake, Yunnan, China. *Engineering Geology*. 2019; 251: 197-213.
[46] N. Ma, G.H. Wang, T. Kamai, I. Doi, M. Chigira. Amplification of seismic response of a large deep-seated landslide in Tokushima, Japan. *Engineering Geology*. 2019; 249: 218-234.
[47] X.M. Fan, C.H. Juang, J. Wasowski, R.Q. Huang, Q. Xu, G. Scaringi, C.J. van Westen, H.B.

Havenith. What we have learned from the 2008 Wenchuan Earthquake and its aftermath: A decade of research and challenges. *Engineering Geology*. 2018; 241: 25-32.
[48] L.H. Tong, B. Qi, H. Ding, C. Xu. Statistical model predicts softening and fluidization induced by vibration in granular materials. *International Journal of Mechanical Sciences*. 2020; 171: 105373.
[49] L.H. Tong, Y. Yu, S.K. Lai, C.W. Lim. Dynamic Weakening of Sandstone Subjected to Repetitive Impact Loading. *Rock Mechanics and Rock Engineering*. 2019; 52(7): 2197-2206.